Incorporation of Fe@Au nanoparticles into multiresponsive pNIPAM-AAc colloidal gels modulates drug uptake and release.

Sulalit Bandyopadhyay[a]†, Marte Kee Andersen[a], Muhammad Awais Ashfaq Alvi[a], Anuvansh Sharma[a], Rajesh Raju[b], Birgitte H. McDonagh[a], Wilhelm Robert Glomm[a,c]†

[a]Ugelstad Laboratory, Department of Chemical Engineering, Norwegian University of Science and Technology (NTNU), N-7491 Trondheim, Norway.

[b]Department of Chemistry, Norwegian University of Science and Technology (NTNU), N-7491 Trondheim, Norway.

[c]Polymer Particles and Surface Chemistry Research Group, SINTEF Materials and Chemistry, N-7465 Trondheim, Norway.

† *Correspondence to: Sulalit Bandyopadhyay (sulalit.bandyopadhyay@ntnu.no), Wilhelm R. Glomm (Wilhelm.Glomm@sintef.no)

ABSTRACT

Here, a synthetic method has been optimized for the synthesis of thermo and pH responsive poly(N-isopropylacrylamide-co-acrylic acid) nanogels which are subsequently loaded with Cytochrome C using a modified breathing-in mechanism. Physico-chemical properties mapped using dynamic light scattering (DLS) and differential scanning calorimetry (DSC) confirm the swelling/de-swelling kinetics as reversible with a volume phase transition temperature (VPTT) of ~ 39 °C. Fe@Au nanoparticles were incorporated inside the nanogel networks using two different methods- coating and in-situ growth. The latter bears closer resemblance to the nanogels only while the former follows the trend of bare Fe@Au nanoparticles. High loading (~96%) and encapsulation (500 µg/mg of nanogels) of Cytochrome C were obtained. Release experiments performed using a dialysis setup and monitored using UV-vis spectroscopy show the highest release at 40°C and pH 3.2 (high temperature, low pH), with maximum release from the Fe@Au coated nanogels that also show a reverse swelling-collapse trend. The location of the drug, incorporation and presence of Fe@Au nanoparticles and drug incorporation method are found to control both the drug release mechanism and kinetics.

KEYWORDS ((Nanogels, core-shell nanoparticles, Volume phase transition temperature, programmed drug release, breathing-in))

INTRODUCTION

Colloidal gels in the nano regime, more commonly referred to as nanogels (NGs), have attracted much attention in drug delivery applications especially for stimuli-responsive release; i.e.; release of cargo molecules under the influence of temperature, pH, ionic strength or other external parameters.[1, 2] NGs refer to swollen nanosized networks formed by physical or chemical cross-linking of hydrophilic or amphiphilic polymer chains.[3] These offer several advantages over conventional drug delivery systems such as liposomes, microspheres, cyclodextrins and so on,[4, 5] not only by providing a finer temporal control over drug release due to their large surface area but also by allowing longer circulation times and targeting properties upon suitable functionalization. Moreover, NGs have been shown to exhibit high loading and encapsulation efficiencies. Although loading efficiency gives an indication of the thermodynamic distribution of the drug, it is not sufficient to indicate delivery vehicle stability against leakage. [6] In this regard, cross-linked NGs are known to provide high encapsulation stability to the drug molecule, rendering them suitable for long term use.[7]

One of the most common methods that has been used for synthesizing thermo-sensitive NGs is precipitation polymerization, named after the fact that the polymer chain - upon reaching a critical length - collapses upon itself, producing pre-cursor particles.[8] This happens above the lower critical solution temperature (LCST) of the polymer.[9] In an aqueous solution, the polymer is in the hydrated state below the LCST, while it becomes hydrophobic above LCST. In a similar way, the cross-linked NGs obtained from this polymer swell in water under a critical temperature and collapse above it. This temperature

is called the volume phase transition temperature (VPTT) of the NG.[10] The transition usually happens over a temperature range instead of a single temperature owing to different crystalline and amorphous domains in the polymer, branching and side-chains, molecular weight distributions among other factors. [11] However, this temperature driven transition allows for release of cargo molecule at a desired rate by fine tuning the physico-chemical properties of the NGs.

Multi-response is introduced in these NGs by incorporating pH-dependent co-monomers. One of the frequently studied temperature and pH-dependent polymeric NGs is that of poly (N-isopropylacrylamide-co-acrylic acid) (pNIPAm-AAc). [12, 13] Although monomer addition, monomer-comonomer ratios can influence the final form of the NGs, the core-shell morphology of the NGs is one of the frequently studied forms. It allows for multiple phase transition behavior with temperature besides adding response to two external stimuli, viz. temperature and pH. The cross-linked NGs also show a tendency of undergoing compression owing to a cross-link gradient in the shell.[8]

Although there exist several synthesis methods to control the size and physico-chemical properties of NGs,[7] pNIPAm-AAc NGs have rarely been investigated to understand their morphological changes under various synthetic conditions and optimize the synthesis process. Moreover, there exists no comprehensive study highlighting the dependence of one synthetic parameter on the other with the primary aim to reduce the size of the gels in the nano regime. The size reduction among other factors is an essential requirement for effective drug delivery applications to avoid phagocytotic sequestration. Recent investigation using poly(acrylic acid) (PAA) nanogels with AuNPs has shown that gels accumulated in the liver and spleen because of their capture by phagocytic cells.[14]

Further, the need to optimize the synthesis route and identify the most important synthetic parameters that influence the properties arises with a growing interest in these NGs towards hyperthermia applications when coupled with magnetic nanoparticles.[15] If the VPTT of these NGs can be maintained higher than the normal body temperature, they can be in the circulation long enough to reach the site of action, where these will collapse owing to hydrophobic change at temperatures above VPTT. A pH responsive release can be utilized in drug delivery in intracellular compartments, such as the late endosomes (pH=5) or lysosomes (pH 4.5-5), or can be tuned to respond to the slightly acidic extracellular fluid surrounding tumors (pH=6.5-7.2). [16] The dual response from both temperature and pH allow controlled release of a drug of interest in response to both the stimuli. In this respect, reversible swelling-collapse behaviour of the NGs determines the probability of repeated cycles of controlled release. However, reversibility of the NGs is a challenge to control owing to different degrees of collapse of the chains and conformational architecture of the polymers. Additionally, incorporation of multifunctionality can also be achieved via coupling NGs with magneto-plasmonic nanoparticles (NPs), whereby introducing imaging and targeting modalities along with stimuli sensitivity in one hybrid system.[17-19]

Here, we report a comprehensive study of the synthesis of pNIPAm-AAc NGs using free-radical emulsion polymerization that show reversible swelling-collapse behaviour. The influence of stabilizer and cross-linker have been investigated to understand the physico-chemical properties of the NGs. In order to incorporate imaging and targeting modalities, the NGs Fe@Au core@shell NPs were incorporated into the NGs using two methods – coating and in-situ growth, resulting in enhancement of drug release properties. The NGs and Fe@Au incorporated NGs were subsequently loaded with a heme protein- Cytochrome

C (Cyt C), a model protein drug- to perform an array of release studies. The effects of both temperature and pH on the release of Cyt C have been studied to determine the dominating factor for release. The effect of drug localization and hybrid composition on the drug release kinetics and mechanisms have been studied. The NGs and their hybrids described herein are promising candidates for hyperthermia applications when coupled with magnetic NPs owing to stability and stimuli programmed release over sustained time periods.

EXPERIMENTAL

Materials and Methods

N-isopropylacrylamide (NIPAm), acrylic acid (AAc) (d= 1.051 g mL^{-1}), Cyt C from bovine heart, sodium dodecyl sulphate (SDS), potassium persulphate (KPS), N, N' – Methylenebis(acrylamide) (BIS), iron pentacarbonyl ($Fe(CO)_5$, 99.99%), octadecene (ODE, 90%), oleylamine (OAm, 70%), chloroauric acid (99.999%), sodium citrate and O-[2-(3-Mercaptopropionylamino)ethyl]-O′-methylpolyethylene glycol (PEG-SH) of molecular weight 5000 Da were purchased from Sigma Aldrich. n-Hexane and hydrochloric acid (HCl 37% fuming) were purchased from Merck Millipore. Sodium hydroxide (pellets AnalaR NORMAPUR® ACS) was purchased from VWR. NIPAm was recrystallized before further use (described below) while the other chemicals were used as received. All solutions were prepared using distilled de-ionized water (MQ water, resistivity ~18.2μΩ-cm) purified by Simplicity® Millipore water purification system which was further purified using 0.45μm syringe filters. Cellulose dialysis tubing (Sigma Aldrich) with a MWCO of 14kDa was used for performing dialysis, both for purification of the NGs and the release studies.

Recrystalization of NIPAm

NIPAm was recrystallized in order to remove impurities that could inhibit the polymerization reaction. The protocol has been adapted and modified from the one reported by Wu *et al*. [20] In a typical recrystallization setup, 5 g of the monomer, NIPAm, was dissolved in 50 mL of n-Hexane at 110°C in a one-necked glass flask equipped with a water condenser and the reaction was run for 2 hours. Thereafter, the flask was directly put into an ice bath for 30 minutes to allow recrystallization of the purified monomer. This solution was then filtered using φ 90 mm filter paper circles, yielding the pure monomer. After drying the purified NIPAm, it was stored at -20°C to prevent absorption of moisture.

Synthesis of pNIPAm-AAc NGs

pNIPAm-AAc NGs were synthesized using free radical emulsion polymerization.[21] A molar compostion of 85 % PNIPAm, 10 % AAc and 5 % BIS was used. [22] In essence, NIPAm (1.6mMoles) and BIS (90.8 μMoles) were put directly into the reactor under nitrogen atmosphere. Thereafter, 10mL of SDS-solution with different concentrations (2 mM, 4 mM, 5 mM, 5.5 mM) was added and the solution left to stir under nitrogen flow for 30 minutes. Prior to addition of the initiator KPS (400 μL of 103.6 mM), AAc (126 μL of 1.46 M) was added into the solution. The reaction was allowed to run for 3 hours. The NG solution was poured into a pre-washed dialysis tube (MWCO 14kDa) and dialysed overnight to remove unreacted monomers and residual reactants.

Synthesis of Fe@Au NPs

Fe@Au NPs were synthesized using a previously reported protocol developed by the authors. [17] In essence, a mixture of ODE (50 mL) and OAm (740 μL) was degassed under Ar atmosphere and vigorous stirring at 120^0C for 30 min. The temperature was raised to

180^0C, following which, 1.8 mL of $Fe(CO)_5$ was injected and the reaction was continued for 20 min. After cooling down to room temperature, the magnetic bar coated with Fe NPs was washed with a 1:2 ratio (by volume) of hexane and acetone. Fe NPs were magnetically separated, washed with acetone and dried in a stream of nitrogen. 5 mg of dried Fe NPs were dissolved in 10 mL of 10 mM sodium citrate solution using sonication at 80^0C for half an hour. Citrate stabilized Fe@Au NPs were synthesized by dropwise addition of 10 mL of 1.5 mM chloroauric acid to the Fe seed NPs under vigorous stirring. The reaction was allowed to run for 20 minutes. Thereafter, the solution was cooled down to room temperature, and Fe@Au NPs were magnetically separated to remove free Au NPs.

PEG coating of the Fe@Au NPs was done using a method reported previously by the authors.[17] Briefly, 2mg of PEG-SH was mixed with 5mg of Fe@Au NPs in a total volume of 5ml MQ water and left to stir for 1 hour. PEG coated Fe@Au NPs were collected by centrifugation.

Incorporation of Fe@Au NPs within NGs

Two different methods were used to prepare combinations of NGs with Fe@Au NPs. The first method was based on post-synthesis coating, while in case of the second method, the NGs were grown atop the Fe@Au seeds via heterogeneous nucleation.

Coating

In order to coat Fe@Au NPs with a representative NG, 3.3 mg of the lyophilized NG was added to 5 ml solution of Fe@Au NPs (concentration of 1mg/ml) and left to stir at 500 rpm for 2 hours. Thereafter, the NG coated Fe@Au NPs were separated using centrifugation at 14,500 rpm for 20 minutes. The sample would be referred to as Fe@Au_NG_c.

In-situ Method

A similar protocol was used as reported earlier for the NGs. A molar composition of 85 % PNIPAm, 10 % AAc and 5 % BIS was used. In essence, NIPAm (0.7 mMoles) and BIS (40.2 μMoles) were put directly into the reactor under nitrogen atmosphere. Thereafter, 1mg of PEG coated Fe@Au NPs and 5mL of 4mM SDS-solution were added and the solution left to stir under nitrogen flow for 30 minutes. Prior to addition of the initiator KPS (200 μL of 210.7 mM), AAc (54 μL of 1.39 M) was added into the solution. The reaction was allowed to run for 3 hours. The NG solution was poured into a pre-washed dialysis tube (MWCO 14kDa) and dialysed overnight to remove unreacted monomers and residual reactants. The sample would be referred to as Fe@Au_NG_i.

Loading of Cyt C

Loading studies of Cyt C were performed primarily with breathing-in mechanism using lyophilisation.[23]. For a typical loading experiment, 20 mg of the freeze dried NG was imbibed with Cyt C solution (10ml, 8.1 μM) and left to stir for 3 hours. Thereafter, the solution was poured into a pre-washed dialysis tube (MWCO 14kDa) and dialysed overnight to remove the unbound Cyt C.

For loading Fe@Au_NG_c with the protein, 5mg of NG coated Fe@Au NPs were imbibed with Cyt C solution (1ml, 8.1 μM) and left to stir for 2 hours. On the other hand, 1.7 mg of Fe@Au_NG_i was imbibed with Cyt C solution (3ml, 40.6 μM) and left to stir for 2 hours Afterwards, Cyt C loaded Fe@Au_NGs were separated from the unbound drug using centrifugation.

Loading efficiencies (L.E., %) and encapsulation efficiencies (E.E., mg drug per mg of NG) of Cyt C were calculated using the following equations.

$$L.E. = \left(\frac{C_{cyt,0} - C_{cyt,t}}{C_{cyt,0}} \right) * 100$$

$$E.E. = \frac{C_{cyt,0} * L.E}{100 * C_{NG}}$$

Where $C_{cyt,0}$ is the concentration (mg/ml) of Cyt C at the start of loading, $C_{cyt,t}$ is the final concentration (mg/ml) of Cyt C after loading, C_{NG} is the concentration (mg/ml) of the NG or NG coated Fe@Au NPs, concentrations of Cyt C being determined using the calibration curve (Figure S1, Supporting Information) or the absorbance method as applicable.

Release studies of Cyt C

After loading NGs with Cyt C, these were subjected to different release media to understand the effect of both temperature and pH on the release kinetics. Three different biologically relevant release conditions were simulated – high temperature (40°C), low pH (3.2) and high temperature along with low pH (40°C, pH 3.4) using MQ water and tuning the pH using different molar ratios of 1M NaOH and 1M HCl. In case of the Fe@Au NPs incorporated into NGs, Cyt C release was monitored only at high temperature along with low pH (40°C, pH 3.4). The release medium was maintained at a temperature slightly above VPTT to account for heat losses during the time study and also to ensure maximum collapse of the NGs.

Characterization techniques

Proton Nuclear Magnetic Resonance (^{1}H NMR)

^{1}H NMR spectra was recorded in a Bruker Advance DPX400 instrument. Lyophilized NG (2 mg) was suspended in D_2O (0.8 ml) and the spectra was recorded with 128 scans at 25 ^oC. The reference peak was locked in, at 4.80 for D_2O. Chemical shifts (δ) were reported in ppm**.**

Scanning (Transmission) Electron Microscopy (S(T)EM)

S(T)EM images were acquired using a Hitachi S-5500 electron microscope operating at 30kV accelerating voltage. TEM images were obtained in bright field mode. TEM grids were prepared by placing several drops of the solution on a Formvar carbon coated copper grid (Electron Microscopy Sciences) and wiping immediately with Kimberly-Clark kimwipes to prevent further aggregation owing to evaporation at room temperature. For studying the temperature effect on the NGs, NG or Fe@Au incorporated NG solutions were heated to 45°C, just prior to placing drops on the TEM grid.

Dynamic light scattering (DLS) and zeta potential measurements

The size distribution and zeta potential of the NGs were measured using a Malvern Zetasizer Nano-ZS instrument, and the manufacturer's own software. All measurements were done in aqueous solutions and results were averaged over triplicate measurements.

Ultraviolet-visible spectroscopy (UV-vis) measurements

UV–vis spectra were acquired with a UV-2401PC (Shimadzu) spectrophotometer. The spectra were collected over the spectral range from 200 to 800 nm.

Differential Scanning Calorimetry (DSC) studies

DSC studies were performed using a TA Instruments Q2000 DSC. The scan rate was 5 °C min^{-1} for both heating and cooling curves and the samples were scanned in the temperature range 5–45 °C. The NG solution was loaded in a Hermetic Aluminium pan while the

reference pan was kept empty. The data were analysed using TA Instruments Universal Analysis 2000 © software.

RESULTS AND DISCUSSION

pNIPAm-AAc NGs with a wide range of sizes and physico-chemical properties were synthesized using free radical emulsion polymerization. Polymerization occurs via homogeneous nucleation, which is initiated by the sulphate radicals generated from the initiator.[24] Common steps of radical propagation and chain growth continue yielding critical polymer chain length. These collapse upon themselves, forming precursor particles. These collapsed particles grow by a combination of the following mechanisms viz aggregation of other precursor particles, by being captured by existing particles, by capturing growing oligoradicals and by monomer addition.[8] A representative ^{1}H NMR spectrum of a representative NG showing that polymerization has proceeded onwards from its precursor (NIPAm) to afford pNIPAm can be found in the Supporting information (Figure S2). The NGs are stabilized by Coulombic repulsion from the charge imparted by the stabilizer (surfactant).

The results obtained for these NGs are sub-divided into the following three subsections that first reveal the size optimization results and their physico-chemical properties, followed by loading and encapsulation efficiencies of Cyt C and finally culminating into the release studies performed under physiological conditions.

Size optimization of the NGs and physico-chemical properties

Size and surface charge of the NGs play a major role in drug delivery applications – NPs smaller than 5.5 nm are removed through renal clearance mechanism while particles larger

than 200 nm are sequestered by phagocytotic cells of the spleen.[25, 26] In the synthetic method described above, among different parameters, the influence of stabilizer (SDS) concentration, cross-linker (BIS) concentration and relative mole ratios of the monomers and cross-linker (NIPAm, AAc and BIS) have been studied. Figure 1 (a) shows the variation of size of different NGs synthesized by modifying the reaction parameters, where the error bars indicate a measure of the polydispersity of the particle distribution. Our results are in close allegiance to those observed by Lyon et al[27], although their group has controlled monodispersity as the most important parameter. Here, we report control of physico-chemical properties of the nanogels as a function of several synthetic parameters outlined in Table 1.

NIPAm (mol %)	AAc (mol %)	BIS (mol %)	SDS (mM)	Size ± PDI (nm)
85	10	5	2.0	593.10 ± 0.10
82	10	8	2.0	376.10 ± 0.10
82	10	8	3.0	309.10 ± 0.02
85	10	5	5.5	182.30 ± 0.10
85	5	10	1.6	378.20 ± 0.03
89	5	6	1.6	415.70 ± 0.02
85	10	5	4.0	412.60 ± 0.07
85	10	5	5.0	231.70 ± 0.06

An increase in the BIS mole percent (from 5 to 8%) causes a substantial decrease in the size of the NGs (A-B), while a coupled increase in the SDS concentration (B-C) causes a

larger collapse above the VPTT, although the decrease in initial size is not sharply evident. This effect can be attributed to a higher cross-linking density, causing a greater collapse.

On the other hand, increasing the SDS concentration from 2mM to 5.5mM (while keeping the BIS mole percent constant) (A-D) causes a dramatic decrease (70%) in the size of the NGs. The main role of SDS is to prevent fusion of hydrophobic nuclei during polymerization.[28] This refers to initial curtailing of the size of the nucleation centres, which further grow by oligomer or monomer addition. A higher initial concentration of SDS provides higher charge stabilization in addition to a denser packing around the incipient nucleation centres, whereby limiting the growth of the NGs owing to electrostatic stabilization. The former (A) shows a volume collapse of ~45% above VPTT while the latter (D) shows a volume collapse of ~95%. This reflects the fact that the hydrophobic tails of the SDS chains interfere constructively in increasing the hydrophobicity of the NGs above VPTT, whereby causing a more efficient collapse.

The mole ratios of the monomer (NIPAm), co-monomer (AAc) and cross-linker (BIS) in the initial reaction mixture also determine the incorporation ratios in the final NGs, whereby effecting their size and collapse properties. In a typical experiment, the mole ratios were varied from 85% NIPAm : 5% AAc : 10% BIS (E) to 89% NIPAm : 5% AAc : 6% BIS (F), while keeping the SDS concentration constant. An increase in the initial size (~10%) is explained through a decreased cross-linking density and reduced charge stabilization from the acidic groups of the AAc blocks. On the other hand, there is a slight decrease (~3%) in volumetric collapse efficiency on increasing the NIPAm content. This might indicate an increase in hydrophobic domains when heated above the VPTT. The effect is aided by a

lower cross-linking density yielding a loosely structured NG thereby needing stronger force to bring together the increased hydrophobic domains during collapse.

The SDS concentration was found to be the most dominating factor determining the size of the NGs. Figure 1(b) shows the variation of the size of the NGs as a function of initial SDS concentration, (error bars indicating polydispersity of particle distribution) while all other parameters were kept constant. As evident from Figure 1(b), the size of the synthesized NGs decreases with an increase in the SDS concentration. The volumetric collapse efficiency - defined as the relative change in volumes of the swollen and collapsed NGs - increases from 45% (2mM) to 95% (5.5mM) with increasing SDS concentration as indicated. As all these concentrations are well below the critical micelle concentration (CMC) of SDS (~8mM at 25°C), [29] we can ignore the tendency of formation of micelles. Moreover, any free SDS is assumed to be completely removed during dialysis. The effect of SDS is summarized as both an increase in the incipient nucleus size, onto which the chains collapse during the synthesis and an increase in the hydrophobicity of the NGs due to incorporation of the hydrophobic surfactant tails (C-12 chains). The initial increase is seen more as an electrosteric stabilization that also explains the lowering of polydispersity while increasing SDS concentrations (Figure 1(a)). On the other hand, incorporation of SDS chains confirms a more efficient collapse above VPTT. This is due to the dominance of hydrophobic interaction forces at increased temperature, coupled with the temperature dependent collapse of the pNIPAm blocks. However, it is worthy of mention that further increase in SDS concentration did not yield smaller NGs and led to temperature driven aggregation when heated above VPTT. Thus, while it is important for the NGs to collapse, it is equally interesting to re-swell them with known efficiency.

Bright field (BF) S(T)EM images of a representative NG at 25°C and NG solution heated just prior to measurement at 45°C are shown in Figures 1(c) and 1(d) respectively. Although the swelling-collapse behavior is difficult to capture in this case, the images show that upon heating the NGs, they tend to associate hydrophobically owing to collapse above VPTT. This effect is synergistically improved due to the presence of cross-linker. Figure 2 provides an overall schematic of the parameters that affect the size of the synthesized NGs.

NGs comprise polymer chains that are cross-linked to each other and their physico-chemical properties are guided by nature of the monomers, their relative composition in the NGs and the degree of cross-linking among others. The swelling-deswelling properties of the NGs are an important aspect for loading and release of biologically relevant cargo molecules like proteins, peptides and nucleic acids. In case of NGs, the cross-linking density among other factors plays an important role in determining the VPTT, collapse rate and gel properties.

Figure 3 (a) shows the variation of the swelling ratio (α) of a representative NG (3mM SDS, 8% BIS) as a function of temperature for a set of heating and cooling cycles. α is defined as $(D/D_0)^3$, where D (nm) represents the hydrodynamic diameter of the NG at any temperature and D_0(nm) represents the diameter of the NG at room temperature. The NGs show a reversible swelling-deswelling transition with a negligible hysteresis. The driving force for aggregation is an increase in entropy from the polymer solution to a two phase system of polymer and solvent. [30] The entropy of a two-phase polymer system and water is greater than a polymer solution owing to a more ordered arrangement of water molecules adjacent to the polymer. The positive entropy change contributes towards aggregation of the polymers, thereby yielding a favourable association (free energy of association is

negative since positive enthalpy change is smaller than the entropy term and does not influence association to a larger extent).[31]

Figure 3(b) shows the variation of size of a representative NG (3mM SDS, 8% BIS) as a function of pH. A remarkable decrease in size (~27%) is observed under acidic conditions. This is in effect due to protonation of the carboxylic acid groups of the poly AAc blocks with an increasing pH. The thermodynamic model developed by Siegel can be used to explain the swelling/deswelling characteristics while changing the pH of the medium.[32] This model considers three sources contributing to the total free energy - (i) NG-solvent system; (ii) NG-solvent mixing, (iii) deformation of polymer networks and osmotic pressure of mobile ions. The NG-solvent mixing component is dominated by the poly AAc segments that undergo dissociation with an increase in pH. Dissociated poly AAc segments are more hydrophilic than non-dissociated segments, whereby a transition from lower to higher pH causes a drastic decrease in the free energy of mixing. Hydrophobic to hydrophilic transition also explains the consequent swelling of the NGs. However, this dissociation is affected by the deformation degree of the polymer network, mostly affected by the cross linking density and the osmotic pressure of OH^- and Na^+ ions. The sharp volume transition that happens at a pH slightly below neutral conditions is reflective of the fact that the pH is high enough to overcome the osmotic pressure, wherein counter-ion-shielding effects occur within the poly AAc domains. [33] Once the osmotic pressure is overcome, a synergistic effect of the favourable free energy of NG-solvent mixing and de-cross-linking of bound poly AAc segments in the domains causes further swelling with increase in pH.

Figure 3(c) depicts the variation of the zeta potential of a representative NG (4.2 mM SDS, 5% BIS) as a function of temperature. The zeta potential not only gives a measure of the surface charge of the NGs but also indicates stability of NGs in solution. A higher surface charge indicates higher stability owing to electrostatic forces. The zeta potential, representative of the charges contributed to by the poly AAc segments, does not change appreciably as a function of temperature. This is due to the fact that zeta potential is only applicable to the NGs in a semi-quantitative manner as some of the charges are buried and contribute partially to the calculated value. Additionally, there exists no well-defined slipping plane between the NG surface and the medium.[34] Herein, the relatively constant zeta potential for the NGs indicates that the poly AAc segments do not show temperature dependence, and their effect in the swelling/deswelling characteristics of the NGs can be widely de-coupled from the effect of the poly NIPAm chains. To further substantiate this, Figures 3(d) and 3(e) depict the changes in size and zeta potential as a function of both temperature and pH for a representative NG (2 mM SDS, 5% BIS). In acidic conditions (pH 3), the collapse of the NGs is substantial owing to charge based interchain repulsion, while in basic medium (pH 9), the NGs do not show much dependence on temperature. In fact, a slight increase in size could point towards aggregation driven by hydrophobic forces. On the other hand, a decrease in the zeta potential of the NGs is observed under acidic conditions, while under basic conditions, the zeta potential does not change much. The increase in cationic charge can be explained by a coupled effect of the collapse of the poly NIPAm segments due to temperature effect and protonation of functional carboxylic groups of the poly AAc segments.

Figure 3 (f) shows a comparison of the sizes of the Fe@Au NPs, a representative NG and Fe@Au NPs incorporated into NGs (Fe@Au_NG_c and Fe@Au_NG_i) as a function of temperature. An increase in the size of the Fe@Au_NG_c NPs as a result of the increase in temperature is observed in contrast with only NG. Although the NG units undergo entropy driven collapse above VPTT, Fe@Au NPs act as crosslinking units (Figure S3, Supporting information) pulling the gelling units together, whereby increasing their effective size as evidenced from their hydrodynamic sizes. On the other hand, FeAu_NG_i resemble the NGs when it comes to temperature driven collapse, showing a volumetric collapse efficiency of 94%, analogous to that of the bare NGs. Thus, the Fe@Au_NG_i behave similarly to the bare NGs, while the Fe@Au_NG_c resemble the characteristics of the bare Fe@Au NPs. However, the increase in size for the Fe@Au NPs (volume increase 36%) may be attributed to aggregation, whereas a 67% volume increase for the Fe@Au_NG_c is mostly due to the cross-linking effect of the Fe@Au NPs that pulls together the already collapsed NG blocks.

This variation in size is further reflected in Figure 3 (g) for Fe@Au_NG_c where the heating and cooling swelling ratio curves diverge from unity with increasing temperature. These structures are much less reversible when compared to NGs alone, since, in addition to chain length, cross-linking density and presence of Fe@Au NPs further affect their size distributions as a function of temperature. For similar reasons, size dependence of NG coated Fe@Au NPs with change in pH, follows a reverse trend. These NG coated Fe@Au NPs are more stable than both the Fe@Au NPs and the NGs themselves owing to higher magnitudes of zeta potential. (Figure S3, Supporting information) Further, the effect of temperature on zeta potential follows a trend opposite to that of the NGs alone. On the other

hand, Figure 3 (h) shows the variation of swelling ratio for Fe@Au_PEG_i as a function of temperature. Although, the heating cooling cycles resemble those of the bare NGs, the hysteresis area is larger. It points to these being less reversible than the bare NGs as a result of different densities of the Fe@Au cores as compared to the NGs. This density difference introduces non-homogeneity in the system properties leading to less well defined swelling-collapse behaviour.

The cross-linked NGs swell under the critical temperature and collapse above it. Thus, the VPTT is an important property of these NGs that determines their biological applications. Figure 4 shows DSC measurements of a representative NG (3mM SDS, 8% BIS) which depicts heat flow during heating and cooling cycles (Figure 4(a),(c) respectively) and specific heat capacity during heating and cooling cycles (C_P) (Figure 4 (b), (d) respectively) as a function of temperature. A gradual transition is seen in all the cases over a defined temperature range and the VPTT is calculated to be at the optimum peak position (heating curves) as ~39° C which is in good agreement with the value calculated using the average of the sigmoidal region of the size-temperature plot (Figure 3(a)). However, VPTT calculated using the cooling curves gives a slightly lower value that can be attributed to a slower re-organization of the polymeric chains in response to an otherwise faster temperature drop rate. This is not the case for the DLS study as there is sufficient time between measurements for the system to reach equilibrium. In case of the NGs coated with NPs, the transitions are not smooth owing to density gradient as a result of inorganic NP incorporation within the matrix. To consider this effect, the VPTT is defined as the temperature where the fraction of the swelled and collapsed states is equal.[35] Using this method, the VPTTs of the NG, Fe@Au_PEG_c and Fe@Au_PEG_i are found to be 37.3 ±

0.2°C, 38.3 ± 0.5°C and 38.9 ± 0.8 °C respectively. Incorporation of the NPs causes an increase in the VPTT as compared to the bare NGs. This is because of an inherent increase of hydrophilicity of the matrix. Among the coated samples, Fe@Au_PEG_i has a higher VPTT. This may be due to different total amounts of NPs incorporated within the matrix or different arrangements of the Fe@Au NPs within the matrix (Figure S3, Supporting Information).

Loading and Encapsulation

The NGs were loaded using breathing-in mechanism where in the freeze-dried NGs or NG coated Fe@Au NPs were imbibed with a concentrated solution of Cyt C. The freeze-dried NGs did not show any change in physico-chemical properties when compared to the as synthesized NGs (Figure S4, See Supporting Information). After the loading step, the free Cyt C was removed using a dialysis tubing (MWCO 14kDa). In case of the NG coated Fe@Au NPs, the free Cyt C was removed using centrifugation.

Cyt C is a highly water soluble heme protein with properties similar to model drug proteins. The heme ligand is located in the lysine rich region of the protein, that imparts a positive charge to the protein at neutral conditions (pI = 10.1, M_w = 12327 Da). [36] It is this front that can interact with negatively charged molecules resulting in complex formation. Coulombic forces between the negatively charged NGs and Cyt C result in the formation of a polymer-protein complex. This results in a release of the counterions associated with the polymer and the protein, causing an entropy gain and thus a net increase in the free energy.[37] Gel swelling yields a lower polymer segment density in the network and greater gel porosity,[34] yielding a higher loading capacity and thus the loading is carried out under

swelling conditions. High loading efficiencies of up to 95% have been obtained for these NGs, with an encapsulation efficiency of ~500 µg per mg of the polymer.

The high loading efficiency can be attributed to the strong interaction between the NGs and the Cyt C under loading conditions. While it is difficult to predict the exact location of the protein inside the NG network, we hypothesize that since the initial binding events of the protein are localized at the surface, a condensation of the particle periphery happens, which limits deeper diffusion of the protein molecule.[34] While the location of the protein influences its interaction with external factors during biological applications, it is ideal when the molecule is closer to the surface and moderately bound to favour release under the influence of external stimuli and/or charge exchange with electrolytes.

In case of the NG coated Fe@Au NPs, loading efficiencies of upto 32% have been obtained with encapsulation efficiencies upto ~14 µg per mg of the Fe@Au NPs. For Fe@Au_NG_i, loading efficiencies of 36.2% and encapsulation efficiencies of 109.7 µg per mg of the nanogel system were observed. The encapsulation efficiency is based on Fe@Au NPs in the former case, while it is based on both the Fe@Au and NGs in the latter case. This means that the efficiencies are not directly comparable as it is difficult to base the calculations on one standard. However, while comparing the loading efficiencies of the systems containing Fe@Au NPs with the bare NGs, there is a drastic reduction in the loading capacity. This is primarily because of lower availability of drug binding sites within the NG, owing to presence of Fe@Au NPs in the nanogel network. (Figure S3, Supporting information)

Release Studies

Cyt C loaded NGs were subjected to different release conditions to monitor their release kinetics. A dialysis setup (Figure S5, Supporting Information) was employed to monitor

the release over time. Three different conditions were chosen to understand their behaviour in response to pH, temperature and a combination of the two. These biologically relevant release conditions were simulated – high temperature (40°C), low pH (3.2) and high temperature along with low pH (40°C, pH 3.4) using MQ water and tuning the pH using different molar ratios of 1M NaOH and 1M HCl. Further, the choice of low pH can be utilized in simulating conditions where drug delivery in intracellular compartments is a matter of concern like in late endosomes (pH=5) or lysosomes (pH 4.5-5). In case of the NG coated Fe@Au NPs, high temperature along with low pH (40°C, pH 3.4) was the only condition used to monitor the release of Cyt C.

Figures 5(a), (b), (c) show the release profiles of Cyt C loaded into the NGs and Fe@Au incorporated NGs using the breathing-in mechanism and/or the traditional method. The traditional method refers to adding a calculated amount of the drug to the NG solutions, whereas the breathing-in mechanism relies on imbibing the freeze-dried NGs with a concentrated drug solution. For the sake of comparison, the concentrations of both the polymers and Cyt C were kept the same for both the methods.

In case of the NGs loaded using the breathing-in protocol, temperature or pH alone is able to cause a release of upto 20% of the loaded Cyt C over a day and no further increase is observed beyond that. A combination of the two effects- low pH and high temperature however yields a cumulative release of upto ~ 40% ranging over two days. Although, a slow release kinetics is observed, this could in effect direct towards long term encapsulation of the carrier molecule inside these NGs, leading to controlled release by variation of the external parameters. Further, the release is assumed to occur by a “squeezing out” mechanism following Fickian diffusion in the initial time period while a combination of

diffusion and degradation of the NGs happens at larger time points. High temperature (above VPTT) and low pH (acidic) conditions enable maximum collapse of the NGs, squeezing out the drug loaded in the porous network.

Comparing the NGs loaded using the breathing in mechanism and the traditional method, a slightly higher release was observed in case of all the release scenarios for the latter method. This can be explained by the fact that the drug molecule is peripherally bound to the NGs while in the case of the breathing-in case, the drug molecule traverses to the inside of the pores and hence requires more time or several stimuli factors to cause substantial release of the cargo. However, it must be noted here that higher loading and encapsulation efficiencies are obtained for the NGs loaded using the breathing-in method. An optimization between the loading capacity and external stimuli affected release of the drug molecule can be used to choose the potentiality of the NGs in the field of drug delivery.

Fe@Au_NG_c shows remarkably rapid release kinetics, releasing almost 55% of the initial loaded drug over a period of ~40 hours in comparison to Fe@Au_NG_i, which exhibits slower release kinetics, bearing closer resemblance to that from bare NGs. It is capable of releasing around 12% over a period of ~50 hours. The higher release in case of Fe@Au_NG_c is due to more peripheral localization of the drug owing to incorporation of the Fe@Au NPs in the NG networks. However, this is not the case for Fe@Au_NG_i, where the drug penetrates deeper into the more open nanogels networks, as also evidenced from S(T)EM images (Supporting Information). A more tortuous path is thus required for the loaded drug to be released, resulting in a slow kinetics. Further, the Fe@Au NPs act as cross-linkers in case of Fe@Au_NG_c, pulling the gelled units closer together, and thereby enhancing ‘squeezing’ out of the drug.

Figures 5(d), (e) and (f) show the plots of ln F as a function of ln t, where F represents the cumulative fraction of the drug released at time t. Majority of the drug release processes from swellable polymer systems are defined by two limiting cases, that is combination of Fickian and Case II transport mechanism. The latter is based on two assumptions- a boundary is formed between the glassy and rubbery phase of the polymer and boundary moves at constant velocity.[38, 39] The overall behavior is defined by combining diffusion-controlled and visco-elastic relaxation-controlled drug release and is given by

$$\mathbf{F = k}t^{n}$$

where, k is the rate constant and n is the diffusional exponent that determines the drug release mechanism. It is observed here that drug release mechanism from the Fe@Au_NG_c and Fe@Au_NG_i is that of super case transport II (n>1) while for the NGs alone are representative of drug release from spherical particles (0.5<n <1) and anomalous in nature. This relates to the conformational arrangement of the NGs which have lesser degrees of freedom in the presence of Fe@Au NPs, leading to less homogeneously defined viscous and elastic regions. On the other hand, different models[40] fitted to the release data yielded a linear dependence of F with t in case of traditionally loaded NGs Fe@Au_NG_c and Fe@Au_NG_i NPs, while they show square root time dependence for NGs loaded with breathing-in mechanism. (Figure S9, Supporting Information) These in conjunction with the diffusional exponent results show that drug incorporation method, location of the drug and presence of Fe@Au NPs largely alter the drug release mechanism and the kinetics. Further, the modulation of release parameters can greatly influence the release kinetics as observed from the release conditions used in the study.

CONCLUSIONS

Synthesis of external stimuli sensitive pNIPAm-AAc NGs has been optimized by varying reaction parameters. Among various parameters that included stabilizer (SDS) concentration, cross-linker (BIS) concentration and mole ratios of reactants, SDS concentration was observed to be the most important parameter to control the size of the NGs – higher concentration of SDS led to smaller NGs. The optimized NGs were used to incorporate Fe@Au NPs in order to incorporate magneto-plasmonic properties to the construct using two methods- coating and in-situ growth.

Under the influence of temperature, the NGs show a reversible swelling/deswelling kinetics, which happens due to an entropically driven expulsion of arranged water molecules. The pH response occurs due to protonation/de-protonation of the AAc blocks. This hydrophilic-hydrophobic transition has been confirmed to be reversible and the VPTT has been determined to be ~ 39°C. The size of the NGs as a function of temperature and/or pH is accounted for by a balance between Coulombic and hydrophobic forces. Fe@Au_NG_i shows a similar temperature based transition. However, an opposite effect is observed for Fe@Au_NG_c which happens as the Fe@Au NPs act as bridge molecules pulling together the gelling units.

Thereafter, Cyt C was loaded into the NGs and Fe@Au incorporated NGs using a modified breathing-in mechanism. This gave high loading and encapsulation efficiencies (~96% and 500µg/mg of NGs, respectively), showing a great capacity to retain drug solution. Using a dialysis setup and three different release conditions, the release kinetics of Cyt C was monitored. The release kinetics has been observed to be rather slow (over several hours), which hints towards their applications in sustained retainment of the encapsulated

molecule. However, high release has been observed under a combination of high temperature (above VPTT) and low pH (acidic) conditions, in which case maximum de-swelling of the NGs is expected, leading to a squeezing release of the drug molecule. The release from Fe@Au_NG_i follows similar kinetics to that of the bare NGs. However, the release of Cyt C from Fe@Au_NG_c is the fastest, accounting for release of almost 55% of the initially loaded drug in ~40 hours. An overall schematic is shown in Figure 6 that describes the release of Cyt C from different configurations of the NG with the Fe@Au NPs. The drug incorporation method, location of the drug, presence of Fe@Au NPs and NP incorporation method largely alter the drug release mechanism. Thus, these temperature/pH programmed NGs can be fine-tuned for both sustained entrapment of cargo molecule and external stimuli directed release of the same by controlling the synthetic parameters and the mode of loading the cargo molecule.

ACKNOWLEDGEMENTS

The authors would like to thank NorFab for financial support in connection to use of NTNU Nanolab and the Faculty of Natural Sciences and Technology, NTNU for financial support.

DISCLOSURE

The authors declare that there is no conflict of interest.

GRAPHICAL ABSTRACT

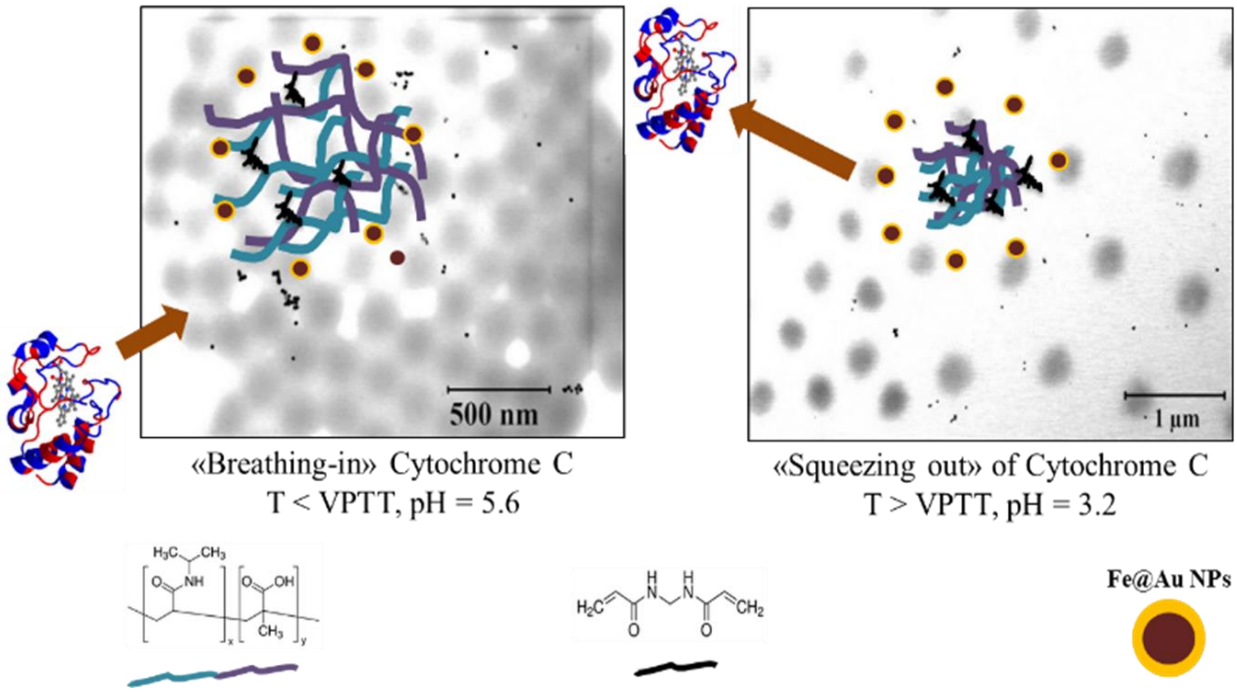

REFERENCES

1. Du, J.Z., et al., *A Tumor-Acidity-Activated Charge-Conversional Nanogel as an Intelligent Vehicle for Promoted Tumoral-Cell Uptake and Drug Delivery.* Angewandte Chemie-International Edition, 2010. **49**(21): p. 3621-3626.
2. Tamura, A., M. Oishi, and Y. Nagasaki, *Enhanced Cytoplasmic Delivery of siRNA Using a Stabilized Polyion Complex Based on PEGylated Nanogels with a Cross-Linked Polyamine Structure.* Biomacromolecules, 2009. **10**(7): p. 1818-1827.
3. Kabanov, A.V. and S.V. Vinogradov, *Nanogels as Pharmaceutical Carriers: Finite Networks of Infinite Capabilities.* Angewandte Chemie-International Edition, 2009. **48**(30): p. 5418-5429.
4. Otero-Espinar, F.J., et al., *Cyclodextrins in drug delivery systems.* Journal of Drug Delivery Science and Technology, 2010. **20**(4): p. 289-301.
5. Matteucci, M.L. and D.E. Thrall, *The role of liposomes in drug delivery and diagnostic imaging: A review.* Veterinary Radiology & Ultrasound, 2000. **41**(2): p. 100-107.
6. Torchilin, V.P., *Structure and design of polymeric surfactant-based drug delivery systems.* Journal of Controlled Release, 2001. **73**(2-3): p. 137-172.
7. Chacko, R.T., et al., *Polymer nanogels: A versatile nanoscopic drug delivery platform.* Advanced Drug Delivery Reviews, 2012. **64**(9): p. 836-851.
8. Nayak, S. and L.A. Lyon, *Soft nanotechnology with soft nanoparticles.* Angewandte Chemie-International Edition, 2005. **44**(47): p. 7686-7708.
9. Wang, X.H., X.P. Qiu, and C. Wu, *Comparison of the coil-to-globule and the globule-to-coil transitions of a single poly(N-isopropylacrylamide) homopolymer chain in water.* Macromolecules, 1998. **31**(9): p. 2972-2976.
10. Constantin, M., et al., *Lower critical solution temperature versus volume phase transition temperature in thermoresponsive drug delivery systems.* Express Polymer Letters, 2011. **5**(10): p. 839-848.
11. Bekhradnia, S., et al., *Structure, swelling, and drug release of thermoresponsive poly(amidoamine) dendrimer-poly(N-isopropylacrylamide) hydrogels.* Journal of Materials Science, 2014. **49**(17): p. 6102-6110.
12. Pelton, R., *Temperature-sensitive aqueous microgels.* Advances in Colloid and Interface Science, 2000. **85**(1): p. 1-33.
13. Wu, X., et al., *The Kinetics of Poly(N-Isopropylacrylamide) Microgel Latex Formation.* Colloid and Polymer Science, 1994. **272**(4): p. 467-477.
14. Chen, Y., et al., *Near-Infrared Emitting Gold Cluster-Poly(acrylic acid) Hybrid Nanogels.* Acs Macro Letters, 2014. **3**(1): p. 74-76.
15. Xiong, W., et al., *Dual temperature/pH-sensitive drug delivery of poly(N-isopropylacrylamide-co-acrylic acid) nanogels conjugated with doxorubicin for potential application in tumor hyperthermia therapy.* Colloids and Surfaces B-Biointerfaces, 2011. **84**(2): p. 447-453.
16. Tannock, I.F. and D. Rotin, *Acid Ph in Tumors and Its Potential for Therapeutic Exploitation.* Cancer Research, 1989. **49**(16): p. 4373-4384.

17. Bandyopadhyay, S., et al., *Synthesis and in vitro cellular interactions of superparamagnetic iron nanoparticles with a crystalline gold shell.* Applied Surface Science, 2014. **316**: p. 171-178.
18. Jafari, T., A. Simchi, and N. Khakpash, *Synthesis and cytotoxicity assessment of superparamagnetic iron-gold core-shell nanoparticles coated with polyglycerol.* Journal of Colloid and Interface Science, 2010. **345**(1): p. 64-71.
19. Zhou, T., B.Y. Wu, and D. Xing, *Bio-modified Fe3O4 core/Au shell nanoparticles for targeting and multimodal imaging of cancer cells.* Journal of Materials Chemistry, 2012. **22**(2): p. 470-477.
20. Zhou, S.Q., et al., *Light-Scattering-Studies of Poly(N-Isopropylacrylamide) in Tetrahydrofuran and Aqueous-Solution.* Polymer, 1995. **36**(7): p. 1341-1346.
21. Slomkowski, S., et al., *Terminology of polymers and polymerization processes in dispersed systems (IUPAC Recommendations 2011).* Pure and Applied Chemistry, 2011. **83**(12): p. 2229-2259.
22. Singh, N. and L.A. Lyon, *Au nanoparticle templated synthesis of pNIPAm nanogels.* Chemistry of Materials, 2007. **19**(4): p. 719-726.
23. Blackburn, W.H., et al., *Peptide-Functionalized Nanogels for Targeted siRNA Delivery.* Bioconjugate Chemistry, 2009. **20**(5): p. 960-968.
24. Ni, H.M., H. Kawaguchi, and T. Endo, *Characteristics of pH-sensitive hydrogel microsphere of poly(acrylamide-co-meth acrylic acid) with sharp pH-volume transition.* Colloid and Polymer Science, 2007. **285**(8): p. 873-879.
25. Chen, L.T. and L. Weiss, *Role of Sinus Wall in Passage of Erythrocytes through Spleen.* Blood, 1973. **41**(4): p. 529-537.
26. Choi, H.S., et al., *Renal clearance of quantum dots.* Nature Biotechnology, 2007. **25**(10): p. 1165-1170.
27. Blackburn, W.H. and L.A. Lyon, *Size-controlled synthesis of monodisperse core/shell nanogels.* Colloid and Polymer Science, 2008. **286**(5): p. 563-569.
28. Smith, M.H. and L.A. Lyon, *Multifunctional Nanogels for siRNA Delivery.* Accounts of Chemical Research, 2012. **45**(7): p. 985-993.
29. Rahman, A. and C.W. Brown, *Effect of Ph on the Critical Micelle Concentration of Sodium Dodecyl-Sulfate.* Journal of Applied Polymer Science, 1983. **28**(4): p. 1331-1334.
30. Schild, H.G., *Poly (N-Isopropylacrylamide) - Experiment, Theory and Application.* Progress in Polymer Science, 1992. **17**(2): p. 163-249.
31. Bromberg, L.E. and E.S. Ron, *Temperature-responsive gels and thermogelling polymer matrices for protein and peptide delivery.* Advanced Drug Delivery Reviews, 1998. **31**(3): p. 197-221.
32. Siegel, R.A., *Pulsed and self-regulated drug delivery* 1990 CRC Press, Boca Raton, FL.
33. Ni, H., H. Kawaguchi, and T. Endo, *Preparation of pH-sensitive hydrogel microspheres of poly(acrylamide-co-methacrylic acid) with sharp pH-volume transition.* Colloid and Polymer Science, 2007. **285**(7): p. 819-826.
34. Smith, M.H. and L.A. Lyon, *Tunable Encapsulation of Proteins within Charged Microgels.* Macromolecules, 2011. **44**(20): p. 8154-8160.
35. Fucinos, C., et al., *Temperature-and pH-Sensitive Nanohydrogels of Poly(N-Isopropylacrylamide) for Food Packaging Applications: Modelling the Swelling-Collapse Behaviour.* Plos One, 2014. **9**(2).

36. Dumetz, A.C., et al., *Patterns of protein - protein interactions in salt solutions and implications for protein crystallization.* Protein Science, 2007. **16**(9): p. 1867-1877.
37. Skobeleva, V.B., et al., *Interaction of hydrogels of acrylic acid-acrylamide copolymers with cytochrome c.* Polymer Science Series A, 2001. **43**(3): p. 315-322.
38. Siepmann, J. and N.A. Peppas, *Higuchi equation: Derivation, applications, use and misuse.* International Journal of Pharmaceutics, 2011. **418**(1): p. 6-12.
39. Brazel, C.S. and N.A. Peppas, *Modeling of drug release from swellable polymers.* European Journal of Pharmaceutics and Biopharmaceutics, 2000. **49**(1): p. 47-58.
40. Barzegar-Jalali, M., et al., *Kinetic analysis of drug release from nanoparticles.* Journal of Pharmacy and Pharmaceutical Sciences, 2008. **11**(1): p. 167-177.

FIGURES

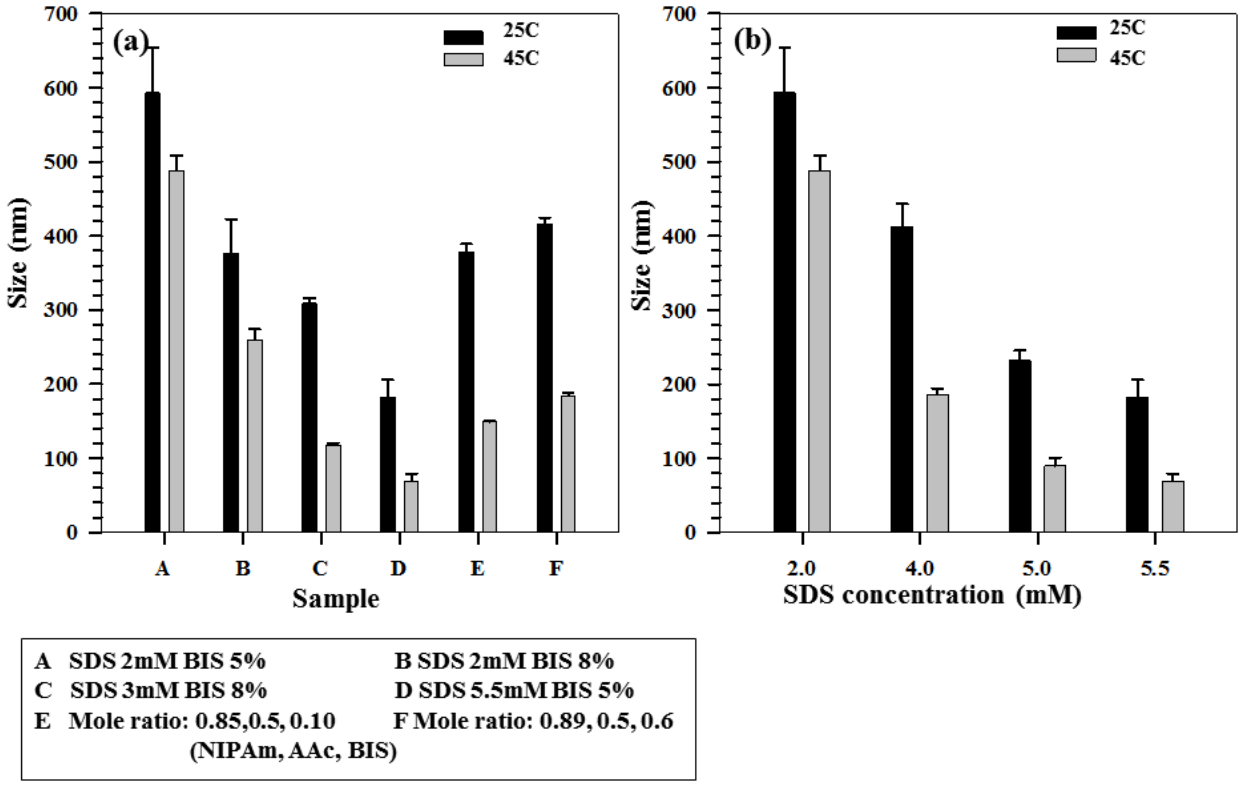

A SDS 2mM BIS 5% B SDS 2mM BIS 8%
C SDS 3mM BIS 8% D SDS 5.5mM BIS 5%
E Mole ratio: 0.85,0.5, 0.10 F Mole ratio: 0.89, 0.5, 0.6
(NIPAm, AAc, BIS)

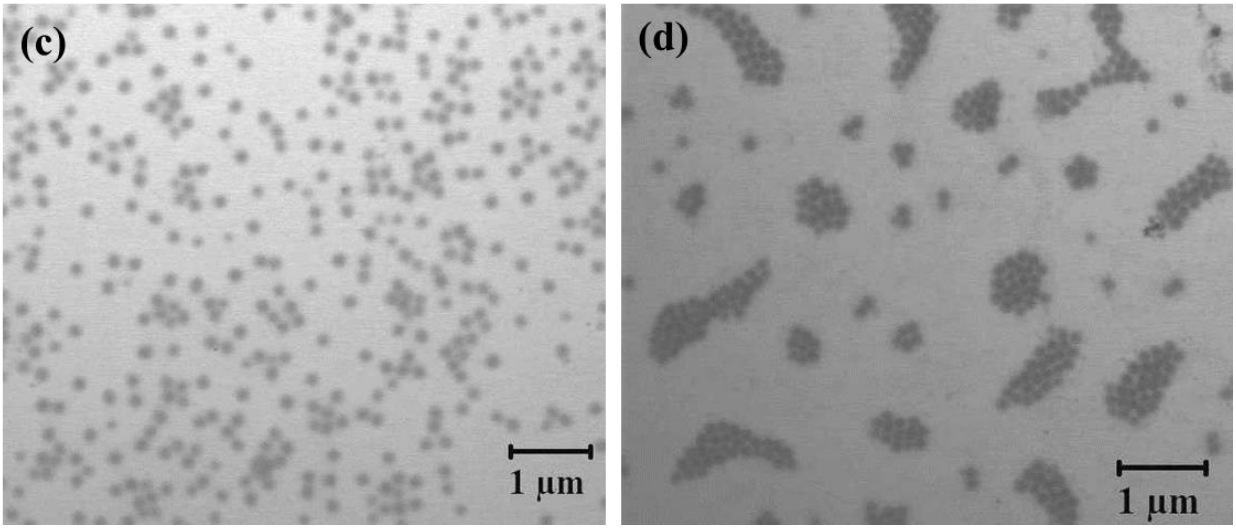

Figure 1 (a) Variation of size of the NGs synthesized using different parameters (b) Variation of size of the NGs as a function of SDS concentration (c) Representative BF S(T)EM image of NGs at 25°C (d) Representative BF S(T)EM image of NGs at 45°C.

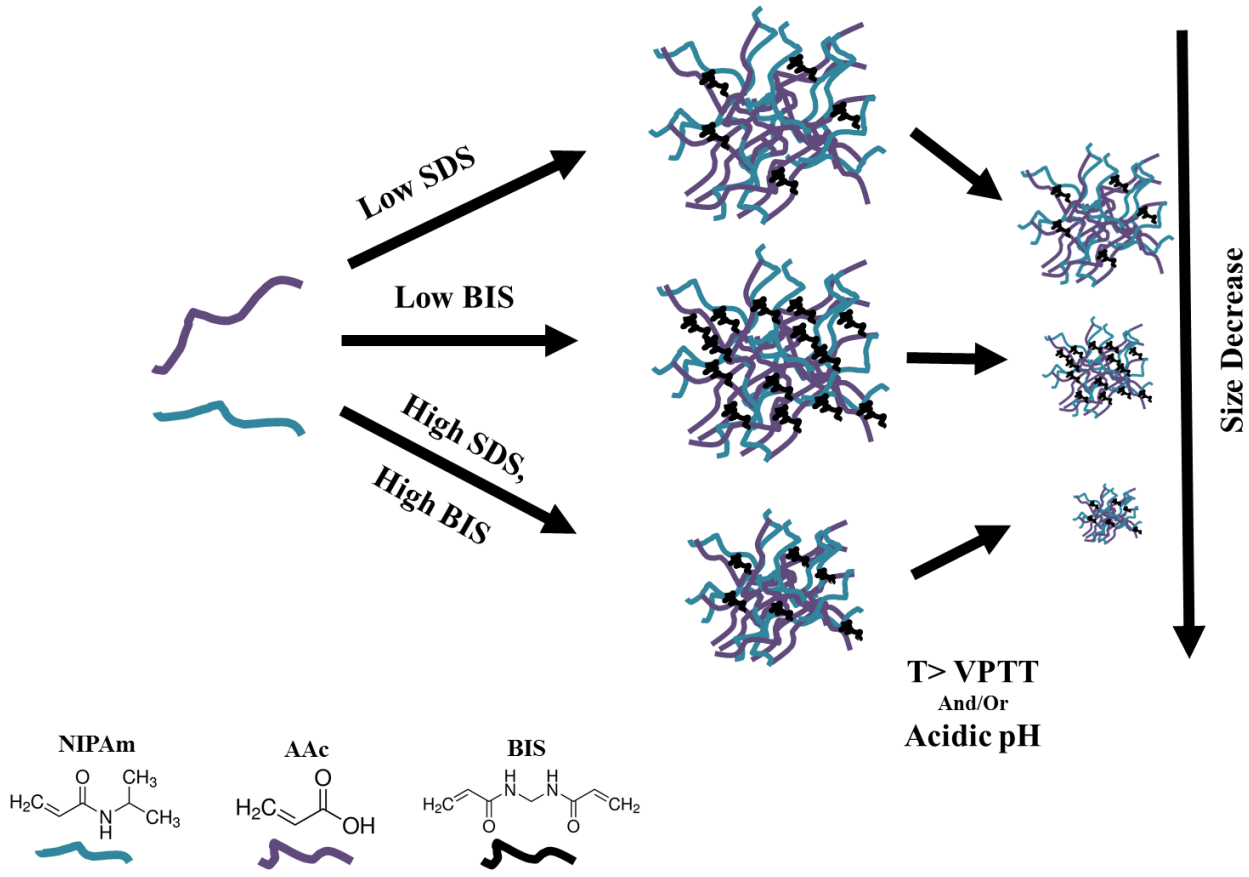

Figure 2 Schematic showing effect of various synthetic parameters on size of pNIPAm-AAc NGs.

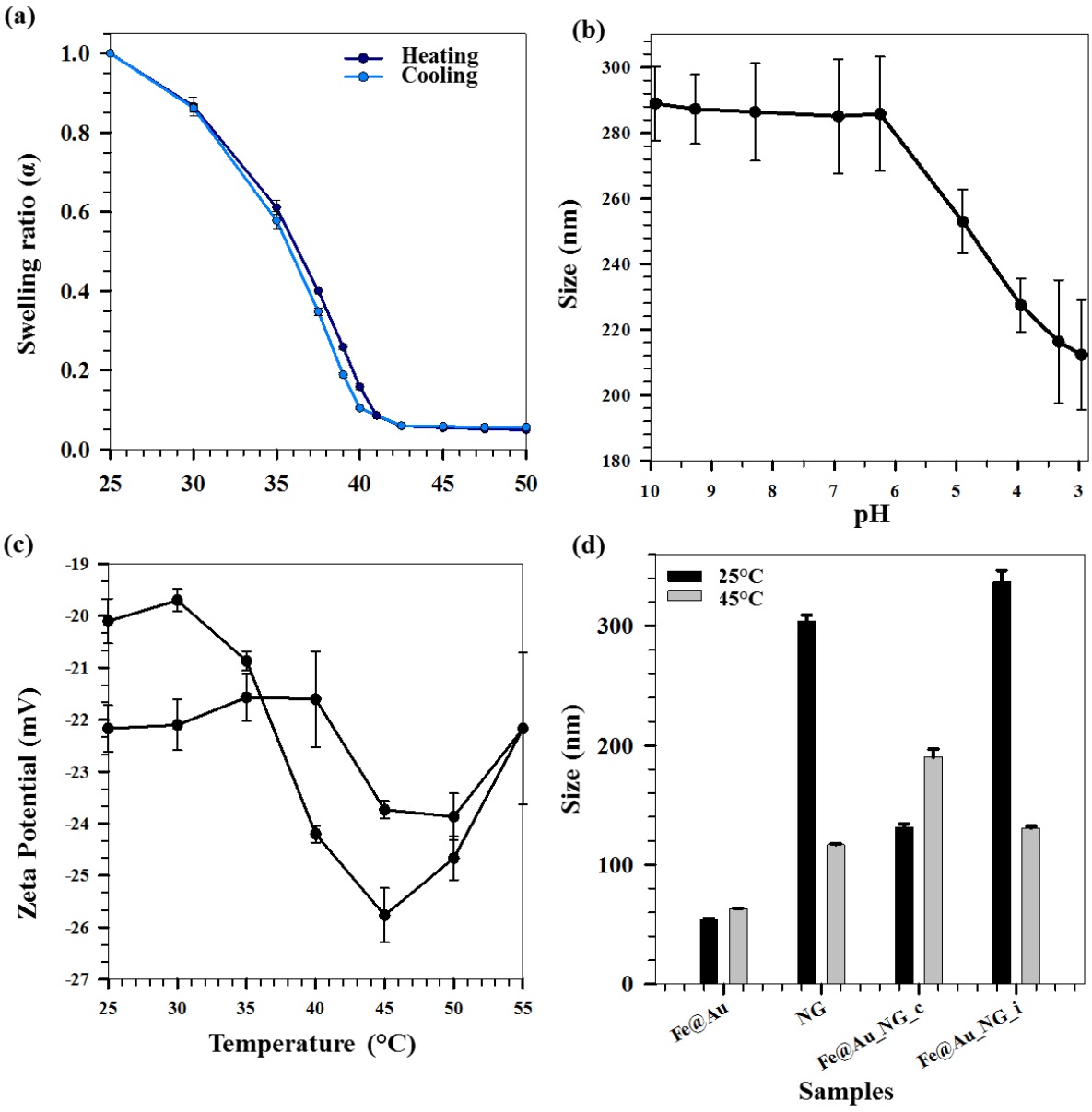
(a)
Swelling ratio (α)
Heating
Cooling
(b)
Size (nm)
pH
(c)
Zeta Potential (mV)
Temperature (°C)
(d)
25°C
45°C
Size (nm)
Fe@Au
NG
Fe@Au_NG_c
Fe@Au_NG_i
Samples

1

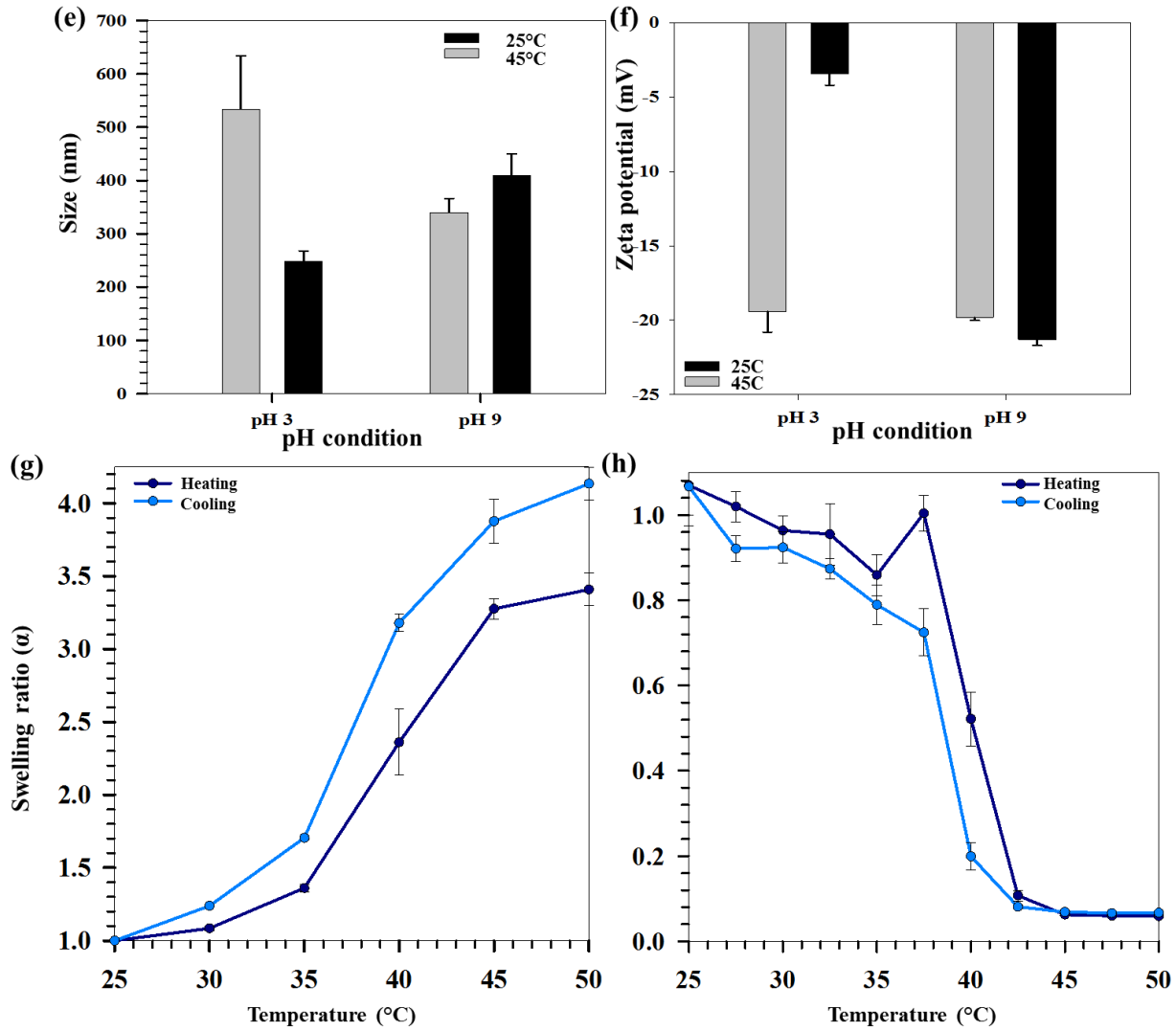

Figure 3 (a) Swelling ratio (α) of a representative NG as a function of temperature during heating and cooling cycles (b) Size of a representative NG as a function of pH (c) Zeta potential of a representative NG as a function of temperature during heating and cooling cycles (d) Size of Fe@Au NPs, representative NG, Fe@Au_NG_c and Fe@Au_NG_i as a function of temperature. (e) Size of a representative NG as a function of pH and temperature (f) Zeta potential of a representative NG as a function of pH and temperature. Swelling ratio of (g) Fe@Au_NG_c NPs and (h) Fe@Au_NG_i NPs as a function of temperature during heating and cooling cycles. The error bars represent standard deviation of a set of triplicate measurements.

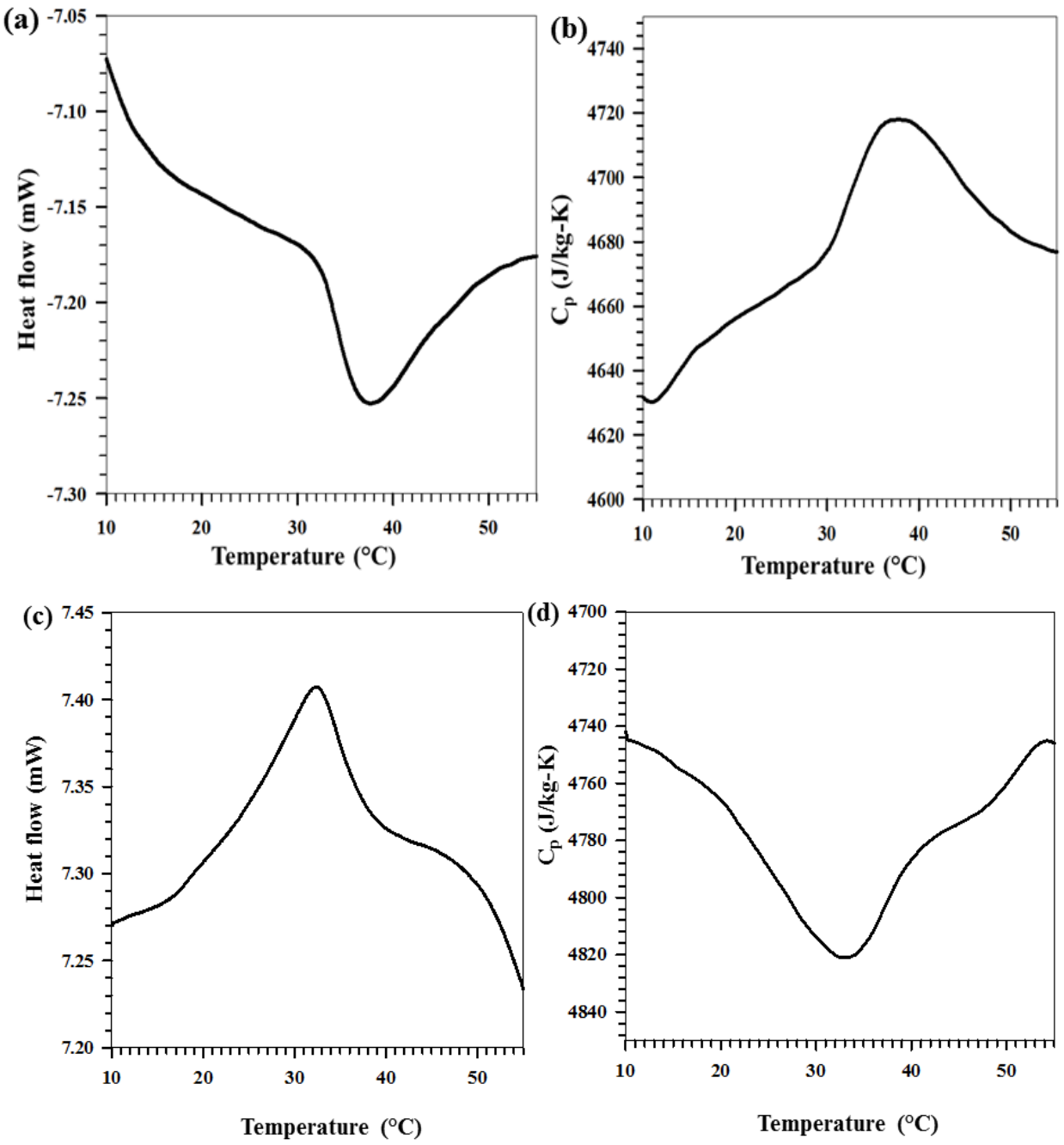

Figure 4 (a) Heat flow (during heating cycle) as a function of temperature for a representative NG (b) Specific heat capacity variation (during heating cycle) as a function of temperature for a representative NG (c) Heat flow (during cooling cycle) as a function of temperature for a representative NG (d) Specific heat capacity variation (during cooling cycle) as a function of temperature for a representative NG.

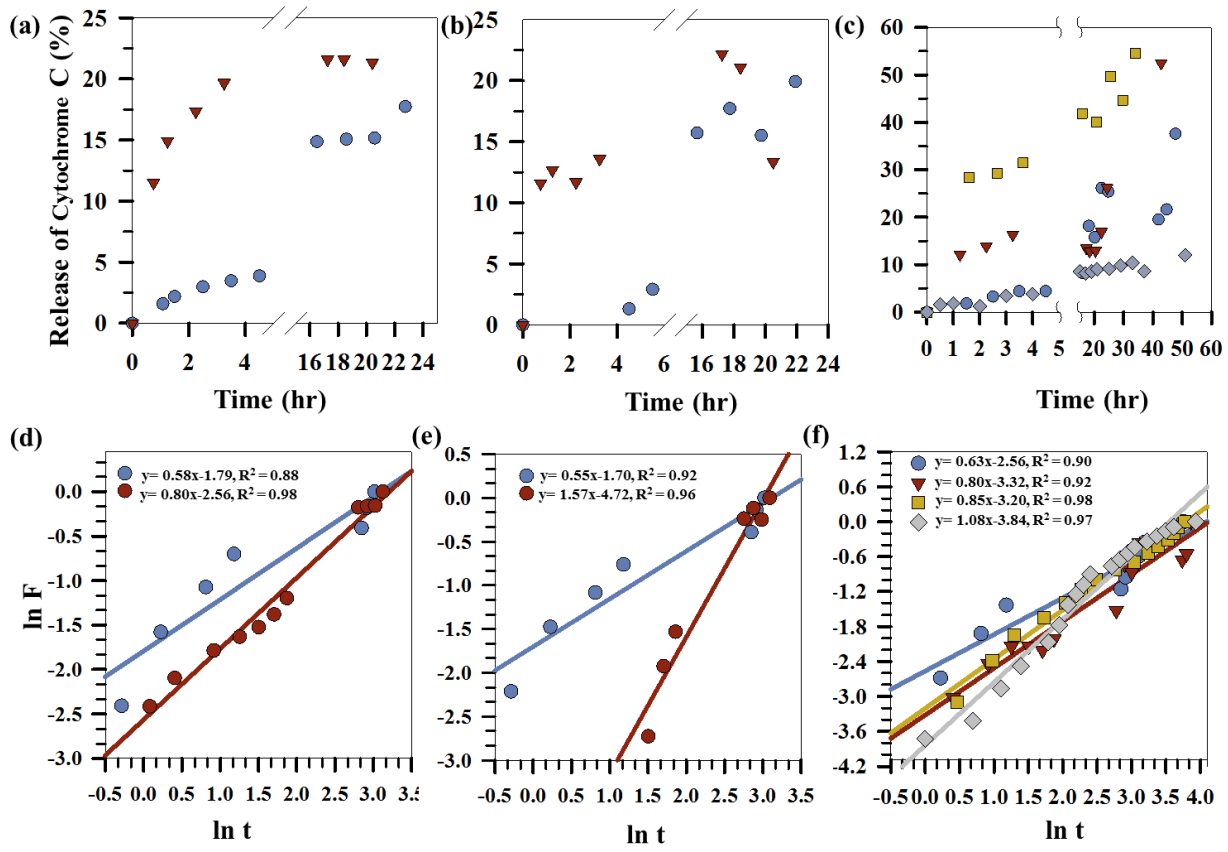

Figure 5 Comparison of release of Cyt C (loaded using breathing-in mechanism and traditional method) over time from (a) a representative NG at pH 3, T 25°C (b) a representative NG at pH 6, T 40°C and (c) a representative NG and NG coated Fe@Au NPs at pH 3, T 40°C. Plots of ln (F) as a function of ln (t) for (d) Case a (e) Case b and (f) Case c above respectively. F represents cumulative fraction of Cyt C.

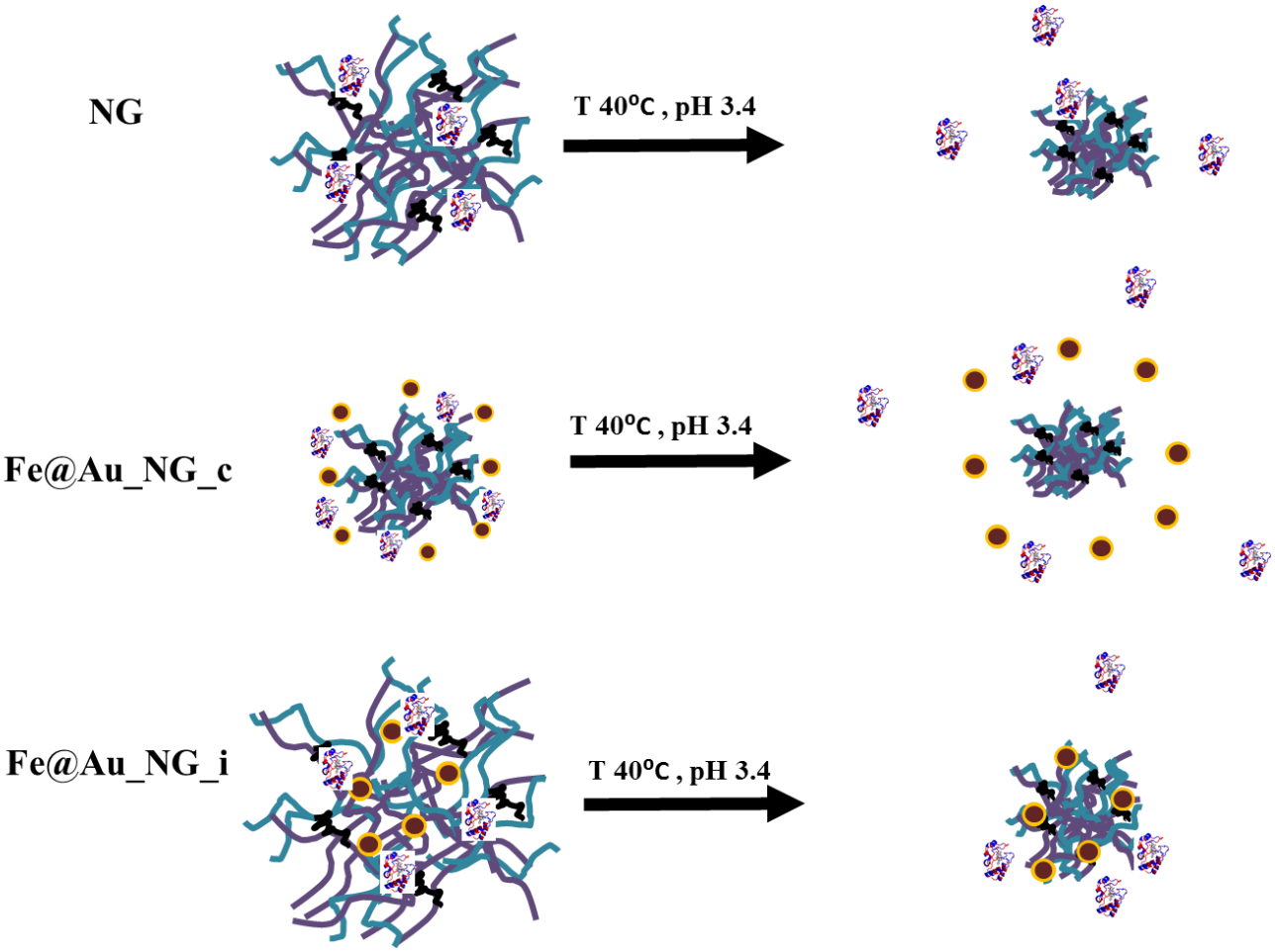

Figure 6 Overall schematic showing release of Cyt-C at pH 3.4 and temperature 40°C from three different NG combinations- NG, Fe@Au_NG_c and Fe@Au_NG_i

Incorporation of Fe@Au nanoparticles into multiresponsive pNIPAM-AAc colloidal gels modulates drug uptake and release.

Supporting Information.

Sulalit Bandyopadhyay[a]†, Marte Kee Andersen[a], Muhammad Awais Ashfaq Alvi[a], Anuvansh Sharma[a], Rajesh Raju[b], Birgitte H. McDonagh[a], Wilhelm Robert Glomm[a,c]†

[a]Ugelstad Laboratory, Department of Chemical Engineering, Norwegian University of Science and Technology (NTNU), N-7491 Trondheim, Norway.

[b]Department of Chemistry, Norwegian University of Science and Technology (NTNU), N-7491 Trondheim, Norway.

[c]Polymer Particles and Surface Chemistry Research Group, SINTEF Materials and Chemistry, N-7465 Trondheim, Norway.

† *Correspondence to: Sulalit Bandyopadhyay (sulalit.bandyopadhyay@ntnu.no), Wilhelm R. Glomm (Wilhelm.Glomm@sintef.no)

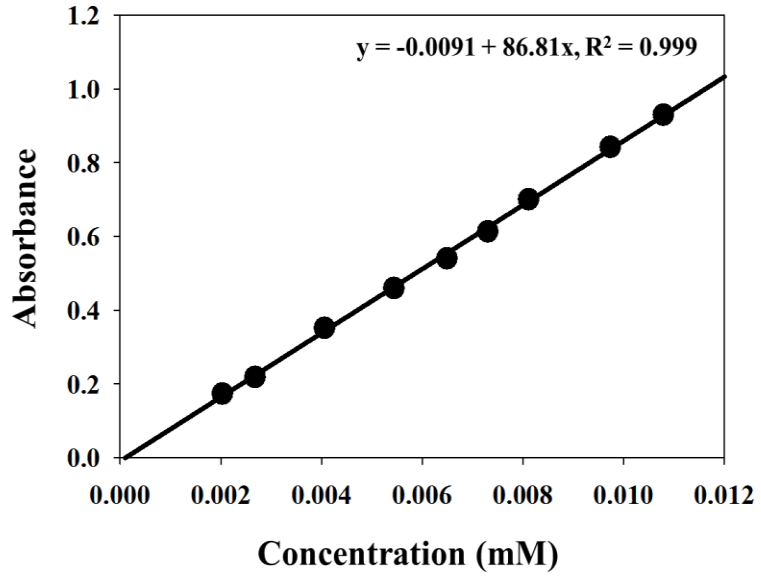

Figure S1 Calibration curve of Cytochrome C

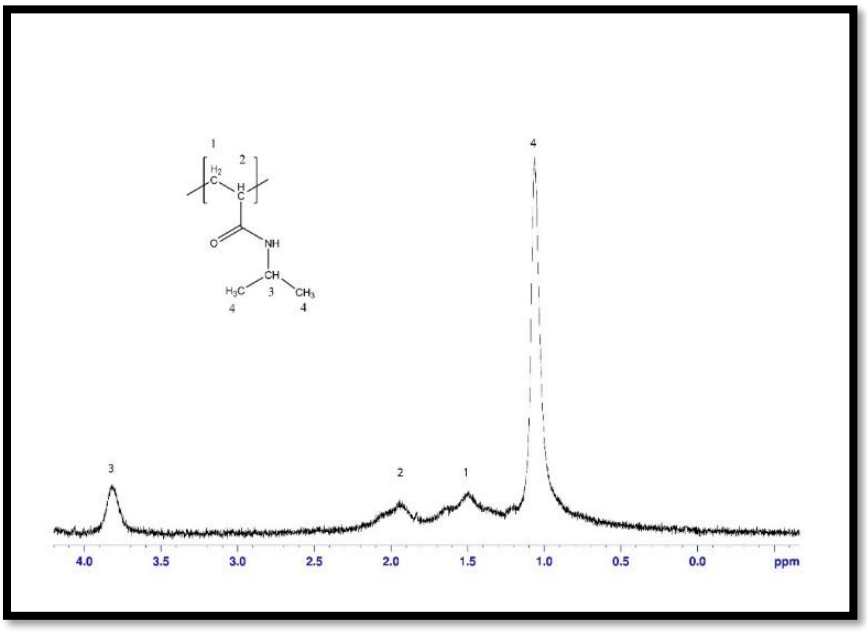

Figure S2 ^{1}H NMR spectrum of a representative nanogel in D20 (400 MHz)

The presence of broad characteristic multiplets at δ =1.95 ppm (-CH2-CH-) and δ =1.51 ppm (-CH2-CH-) along with broad singlets at δ =1.05 ppm (CH3-CH-CH3) and δ =3.85 ppm (CH3-CH-

CH3) indicates that polymerization has proceeded onwards from its precursor (NIPAm) to afford nanogels.

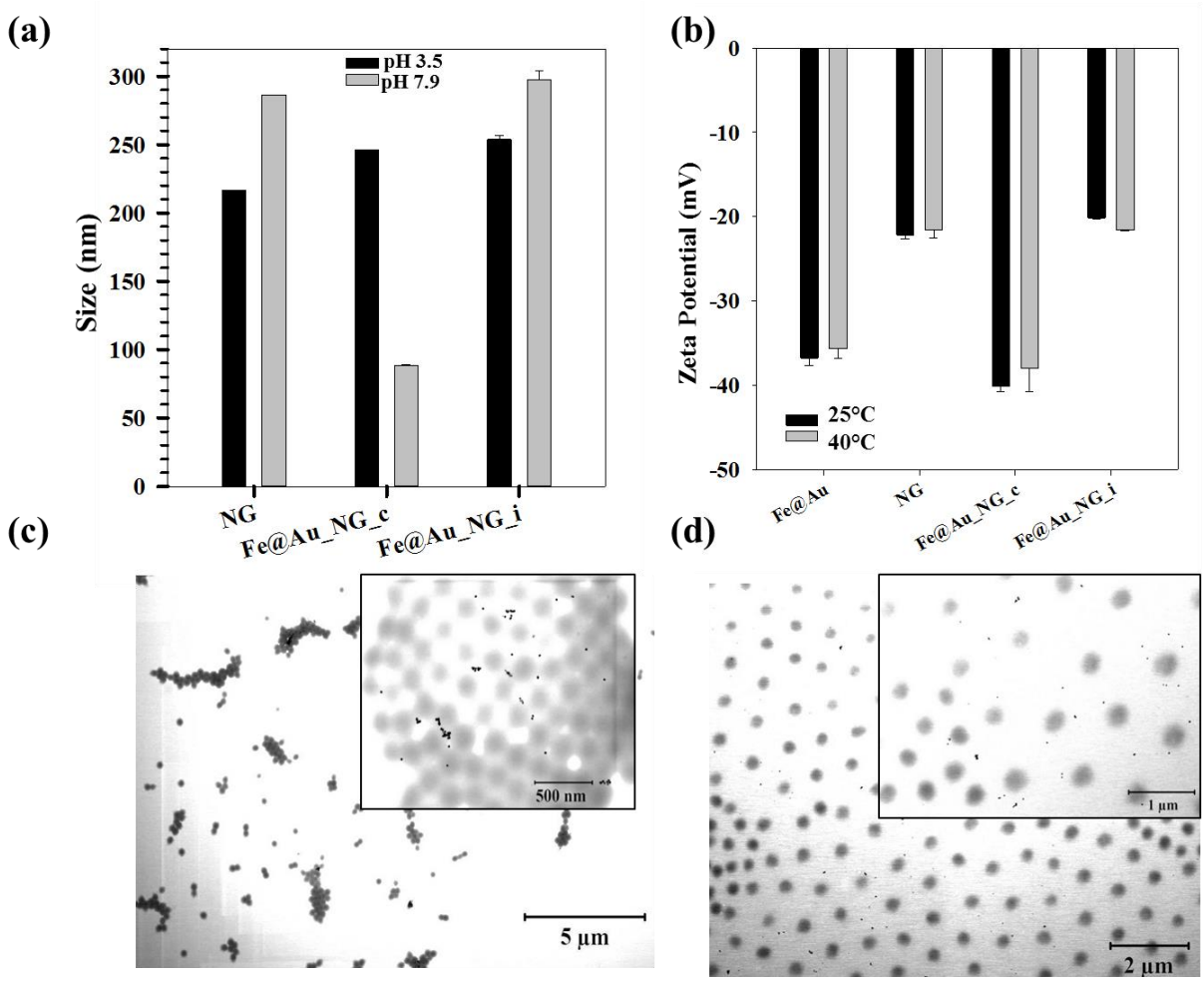

Figure S3 (a) Variation of size of NG, Fe@Au_NG_c, Fe@Au_NG_i with pH (b) Comparison of zeta potentials as a function of temperature for Fe@Au NPs, a representative nanogel and Fe@Au_NG_c and Fe@Au_NG_i Representative BF S(T)EM image of Fe@Au_NG_c (c) at 25°C and (d) at 45°C respectively. Red circles show Fe@Au NPs

1

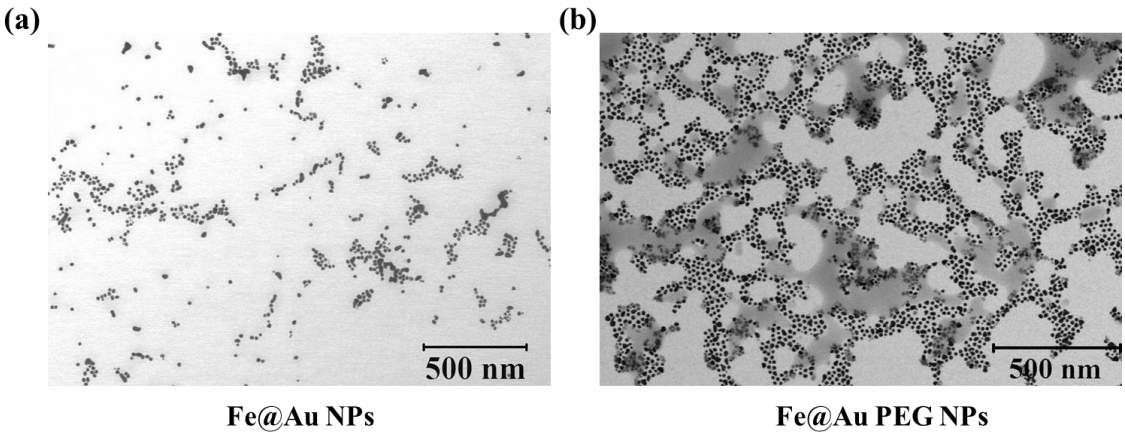

2

3 Figure S4 Representative S(T)EM image of (a) Fe@Au NPs and (b) PEG coated Fe@Au NPs.

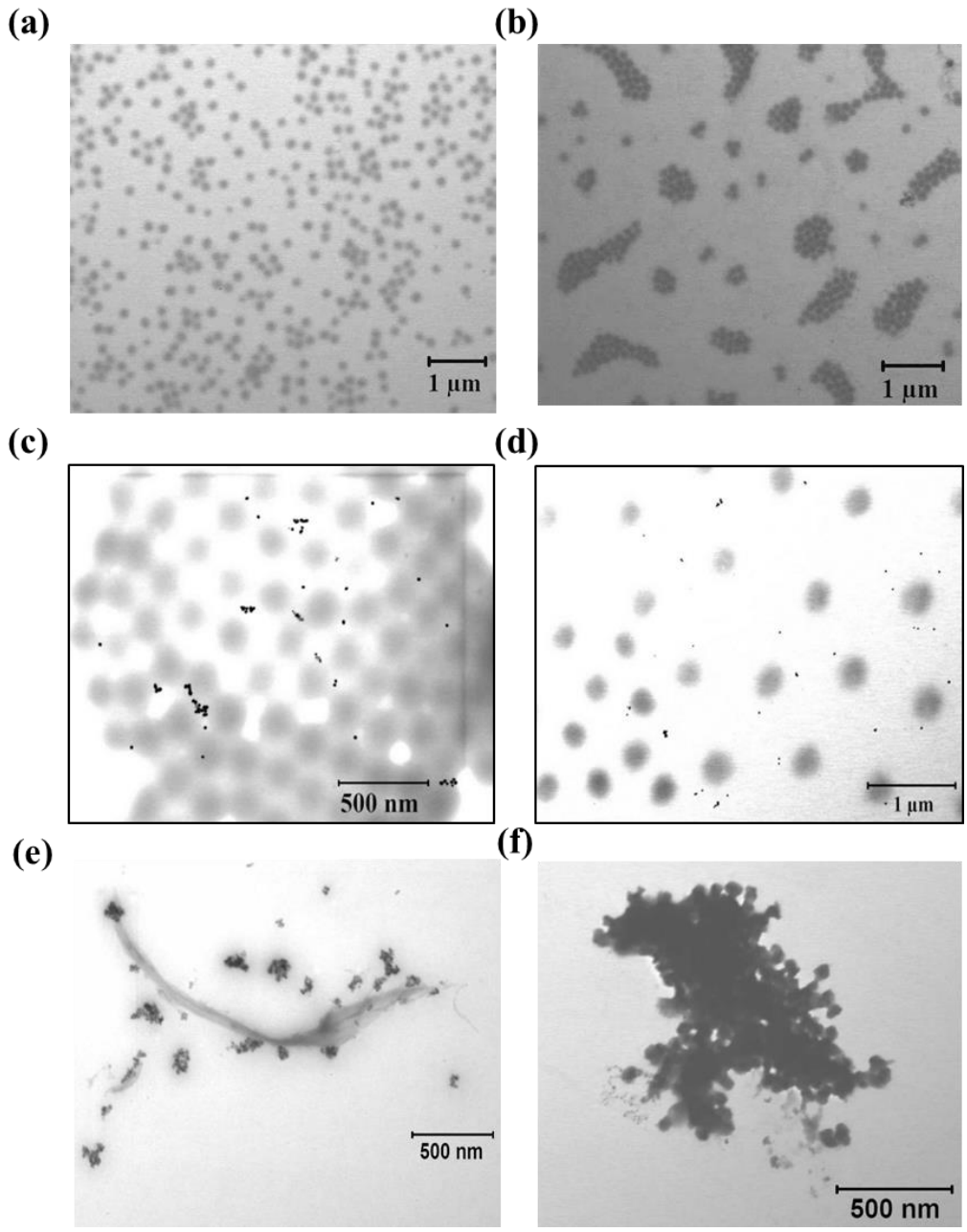

Figure S5 Representative S(T)EM images of (a) a representative nanogel at 25°C (b) at 45°C (c) Fe@AU_NG_c at 25°C (d) at 45°C (e) Fe@Au_NG_i at 25°C and (f) at 45°C respectively.

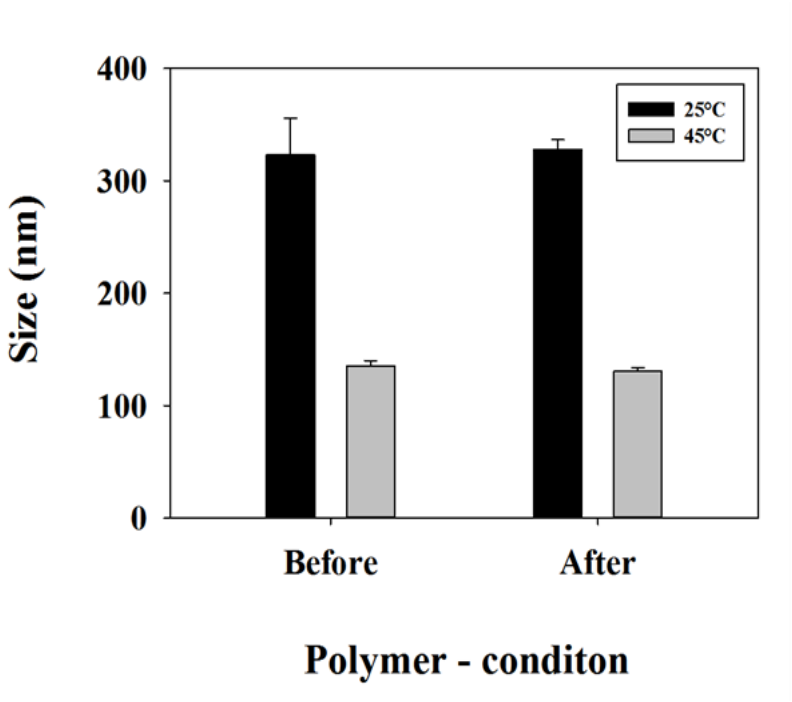

Figure S6 Variation of size of a representative nanogel before and after freeze drying

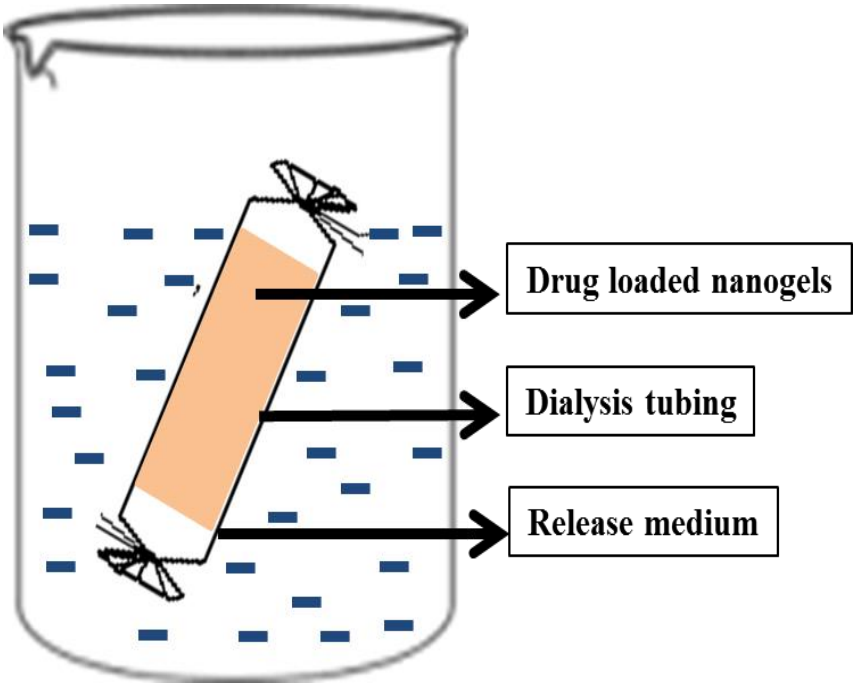

Figure S7 Schematic of the dialysis setup used for studying release from the nanogels.

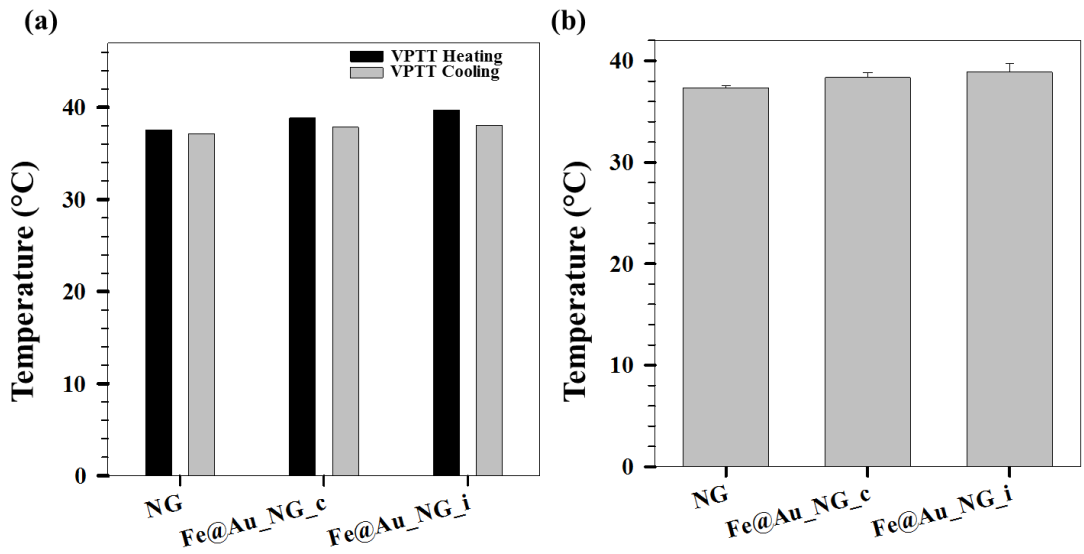

Figure S8 (a) Heating and Cooling VPTTs and (b) Average VPTTs for representative nanogel, Fe@Au_NG_c and Fe@Au_NG_i respectively.

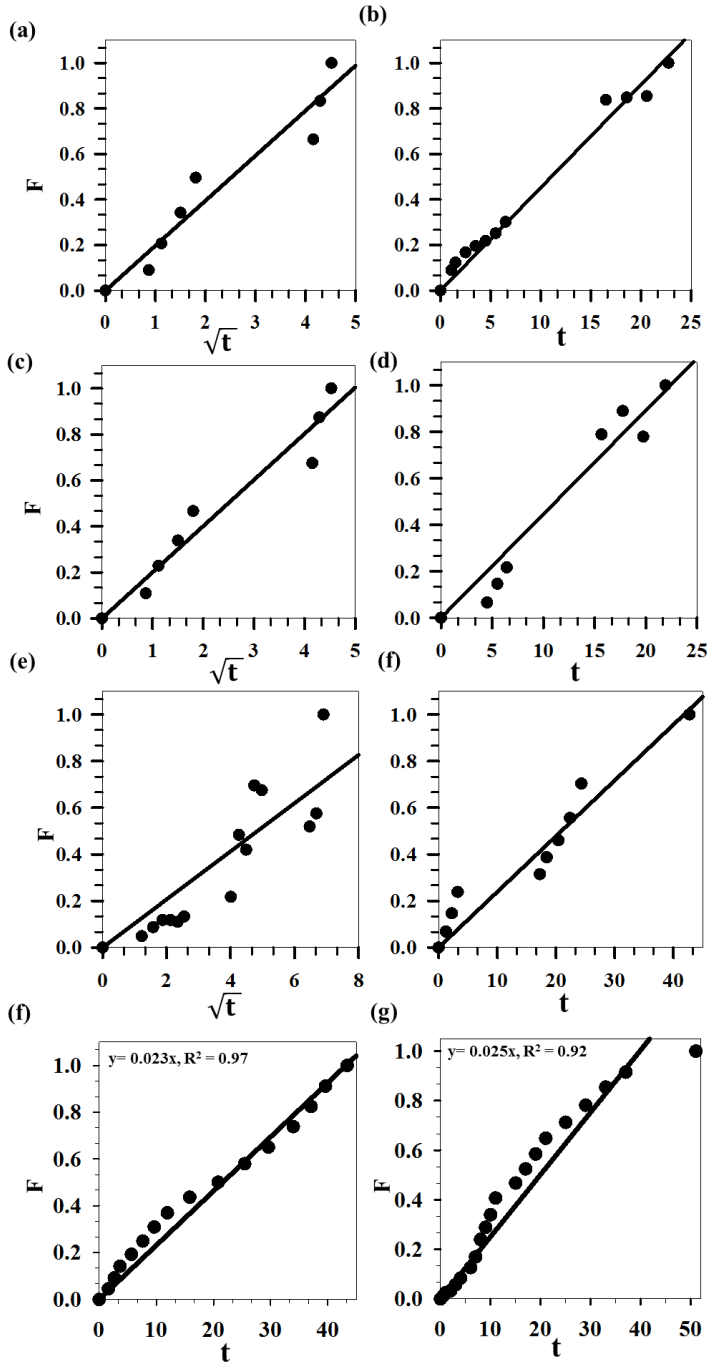

Figure S9 Fitted model for nanogel loaded with Cytochrome C (a) using traditional method and release monitored at 25C and pH 3 (b) using breathing in method and release monitored at 25C and pH 3 (c) using traditional method and release monitored at 40C and pH 6 (d) using traditional method and release monitored at 40C and pH 3 (e) using breathing in method and release monitored at 40C and pH 6 (f) using breathing in method and release monitored at 40C and pH 3

(g) Fitted model for Fe@Au_NG_i loaded with Cytochrome C using breathing in method and release monitored at 40C and pH 3